Sci

MDPI

Article

A Novel Nonlinear CPG-Based Oscillator Model for Quadruped Robotic Locomotion

Edgar-Mario Rico-Mesa [1,*,†] and Jesus-Antonio Hernandez-Riveros [2,†]

[1] Servicio Nacional de Aprendizaje, SENA, Medellín 050042, Colombia
[2] Universidad Nacional de Colombia, Medellín 050034, Colombia; jahernan@unal.edu.co
* Correspondence: emrico@sena.edu.co
† These authors contributed equally to this work.

Abstract

In recent decades, robotic locomotion has applied different techniques to emulate central pattern generators (CPGs). The theory of CPG explains the biological functions of motor control in living organisms. This paper presents an unpublished model for coupled nonlinear oscillators. This model employs a canonical nonlinear differential equation system to coordinate joint activity. The analysis, conducted under the criteria of chaos and bifurcation theory, determines that the new model is successful and without the presence of chaos. The new model is compared with other cases, including the Wilson–Cowan, Hopf, and Van Der Pol models, as well as with the operability of different robots. It highlights the new model's advantages in terms of versatility, simplicity, and processing, as well as the comparisons of metrics of locomotion, such as support factor and symmetry index between hemibody metrics. The new model is applied to the locomotion of two quadruped robots (a crab and a dog) used in research on transitions between types of locomotion, considering both physical and computational limitations.

Keywords: central pattern generators; nonlinear differential equations; locomotion; coupled oscillators; articulated robotic systems

Check for updates

Academic Editors: Huosheng Hu and Jose Luis Sanchez-Rojas

Received: 13 May 2025
Revised: 27 January 2026
Accepted: 30 January 2026
Published: 5 February 2026

Copyright: © 2026 by the authors. Licensee MDPI, Basel, Switzerland. This article is an open access article distributed under the terms and conditions of the Creative Commons Attribution (CC BY) license.

1. Introduction

Locomotion in living beings has evolved according to the demands of the environment with which they interact [1]. Therefore, the locomotion of terrestrial quadruped and biped animals has been studied in depth by different biologists [2]. However, in the evolution of robotics, humans have worked intensively on locomotion mechanisms for artificial systems, among the most perfected are mobile robots on flat surfaces through solutions with wheels [3]. In irregular terrain, artificial wheeled mobile systems are limited, which has led to the implementation of biped, quadruped, and hexapod systems that perform better on these surfaces [4]. Biologists describe the signals that govern locomotion behavior from the nervous central system and the function of the brain, such as central pattern generators. So, central pattern generators (CPGs) are involved in the refinement of the response of animals on uneven terrains of great complexity [5]. Now, transferring these results to robots with legs is a trend [6]. Neural oscillators simulate the biological signals of locomotion in quadruped robots. Consequently, this work aims to develop a model for oscillators that play CPG. Initially, specific cases of oscillators have been developed seeking mathematical schemes that allow the application of central pattern generator theory in quadrupedal robotic systems. The mathematical schematics (systems of differential equations) are

analyzed to consolidate their oscillator construction model. The new model of systems of equations represents a range of neural oscillators between two to six neurons. It analyzes specific cases of systems of differential equations or neuronal oscillators defined from the canonical mathematical new model, subject to the criterion of chaos and bifurcation theory. The new model is compared with other models such as Wilson–Cowan, Hopt, and Van Der Pol, used in similar research, finding aspects of versatility, simplicity, and processing in favor of the new model. Robotic applications are also compared by analyzing their locomotion behavior through metrics such as support factor and symmetry index, highlighting that the proposed model is pertinent when hardware has limited computing power and joint torque.

The sections in this paper are as follows.

Section 2: This section presents theories such as central pattern generators, which explain the behavior of motor functions in living beings from a biological perspective; chaos and bifurcation theory, which analyzes the stability of dynamic systems; and a brief review of locomotion control techniques in four-legged articulated robots.

Section 3: This section presents a new mathematical model for constructing nonlinear oscillators that reproduces the behavior of central pattern generators. The chaos and bifurcation theory, the criteria that study the dynamic behavior of specific cases of systems of differential equations, reports that simulated responses exhibit transients that stabilize into oscillations, and the bifurcation/chaos analysis (including time histories, phase diagrams, Poincaré maps, and FFT) indicates closed, stable orbits without signs of bifurcation in the examined ranges. The section also includes experimental verification in two quadruped cases, applying systems derived from the general model (two, three, and four equations) for locomotion control. The locomotor response of the two quadruped cases is presented through metrics (support factor and the symmetry index between hemibodies).

Section 4: This section compares the results obtained with oscillators created using the new mathematical model with reports from similar works presented in the brief review of the literature. The new model is compared with other models, such as Wilson–Cowan, Hopt, and Van Der Pol, used in similar research, and it is found to have aspects of versatility, simplicity, and processing that favor the new model. Robotic applications are also compared in terms of metrics used for locomotion, such as support factor and index of symmetry between hemibodies, highlighting the relevance of the proposed model when hardware has limited computing power and joint torque.

2. Current Research and Methods

This work aims to verify the stability of the dynamic system configured as neural oscillators in the cases developed from the model. In addition, a tracking of similar works in locomotion is done. This type of dynamic system enables the development of a biological procedure for locomotion in an artificial system called a central pattern generator (CPG).

2.1. Central Pattern Generators (CPGs)

CPGs are a theory investigated in the second half of the 20th Century by biologists like Grillner in [7] and Marder in [8]. Central pattern generators are neural circuits that produce voluntary and involuntary rhythmic motor patterns. The motor patterns include walking, breathing, flying, swimming, and others. This pattern requires little specific time information obtained from sensory inputs. In the 21st Century, CPGs have been applied in artificial intelligence projects to optimize locomotion, increasing the reliability and performance of robotic systems such as bipeds, quadrupeds, and hexapods in space exploration [9]. The terrestrial displacement in living beings is executed voluntarily from the main nervous organ of the central system (brain). The basic movements (patterns)

happen in the spinal cord. Graham Brown proposed this presumption in 1911 [10]. The classic CPG model relies on two mutually inhibitory "half centers", both under tonic excitation [11]. This oscillation causes alternating flexion and extension of the extremities. Neural networks are connected via synapses (inhibitory and excitatory connections). The link between neurons (Figure 1) generates a rhythmic firing (CPG).

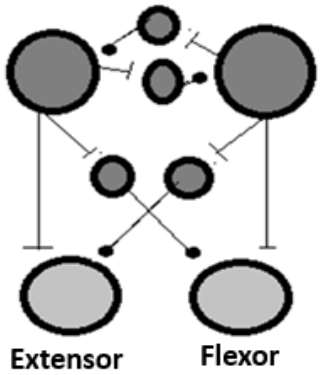

Figure 1. CPG model classic (half-center model) in mammals.

According to Crook [12], the periodic electric explosions in the ventral roots are induced displacements. These signals arise in each segment of the spinal cord. Therefore, a proposal oscillator mathematical model of two and four neurons with excitation signals reproduces the oscillatory movement (Figure 2).

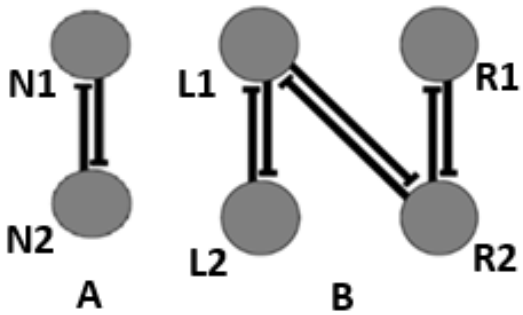

Figure 2. Oscillator architecture. (**A**) Two neurons, (**B**) four neurons.

These models are simple enough to be analyzed mathematically but very complex to capture some of the basic principles that govern the behavior of a network of two oscillators and four oscillators. Rand, Cohen, and Holmes propose Specific mathematical models [12] for a network of two and four oscillators, where each one is a simple biological oscillator, without considering the structure of the oscillator and the mechanisms that they produce it (Equations (1)–(6)).

Two neurons:

$$\dot{\theta}_1(t) = w_1 + h_{12}(\theta_1, \theta_2) \tag{1}$$

$$\dot{\theta}_2(t) = w_2 + h_{21}(\theta_2, \theta_1) \tag{2}$$

Four neurons:

$$\dot{\theta}_1(t) = w_1 + h_{12}(\theta_1, \theta_2) \tag{3}$$

$$\dot{\theta}_2(t) = w_2 + h_{12}(\theta_1, \theta_2) + h_{23}(\theta_2, \theta_3) \tag{4}$$

$$\dot{\theta}_3(t) = w_3 + h_{32}(\theta_3, \theta_2) + h_{34}(\theta_3, \theta_4) \tag{5}$$

$$\dot{\theta}_4(t) = w_4 + h_{43}(\theta_4, \theta_3) \tag{6}$$

where $h_{ij}(\theta_i, \theta_j)$ represents the periodic coupling effect between the j_{th} oscillator and the i_{th} oscillator.

2.2. Chaos and Bifurcation Theory

A dynamical system is the mathematical description of a deterministic process, meaning that the future and past states of the process are predicted mainly by knowing its current state and the conditions under which it evolves. If conditions do not change over time, the behavior of such a system could be considered completely defined by its initial state.

A dynamical system is typically expressed mathematically based on derivatives or integrals (Equation (7)), which leads to its behavior being nonlinear [13]. A continuous time dynamical system is a system of equations that has the following definition [14]:

$$\dot{x} = f(x, t, u, p) \tag{7}$$

where

- $\dot{x}$: is the time-derivative of the state;
- $x \in R_n$: is the state;
- $t \in R$: is the time;
- $u \in R_m$: is the input;
- $p \in R_q$: are the parameters;
- f: is the vector field.

When a slight change in a parameter results in a significant change in the graph's topology, a bifurcation is observed in a dynamical system. The change's value is called the bifurcation point [13].

A bifurcation point is a point $\bar{p}$ in the parameter space where $f(x, p)$ is not structurally stable. A system $f(x, p)$, with parameters $p \in R_q$ is structurally stable if its flow is topologically equivalent to the flow of all systems $f(x, p')$ with p' in a neighborhood of p.

The eigenvalue criterion establishes the stability of nonlinear systems with $J_f(x)$ as the Jacobian of a vector field $f(x)$ concerning the state x, and let $\bar{x}$ be the point of equilibrium.

If all eigenvalues of $J_f(\bar{x})$ have a negative real part, then the equilibrium $\bar{x}$ of the nonlinear vector field $f(x)$ is asymptotically stable. If at least one of the eigenvalues of $J_f(\bar{x})$ has a positive real part, then $\bar{x}$ is unstable. In linear systems, the largest Lyapunov exponent equals the real part of the eigenvalue with the largest absolute value. In contrast, in nonlinear systems, Lyapunov exponents can be calculated using numerical methods, such as Gram–Schmidt orthogonalization [14].

2.3. Metrics

2.3.1. Duty Factor (β)

The duty factor quantifies the fraction of the gait cycle in which a limb remains in contact with the ground (support phase). It is defined for each leg and each cycle as:

$$T = T_{support} + T_{air} \tag{8}$$

$$\beta = \frac{T}{T_{support}} \tag{9}$$

In locomotion biomechanics, β is used as a spatiotemporal descriptor to distinguish gait regimes and compare patterns across conditions (speed, surface, control strategy). Recent studies have formally used the duty factor to characterize lower limb kinematic differences between groups with high and low β across a range of running speeds, reinforcing its usefulness as a compact metric to more easily understand the configuration of the stance and air phases within the locomotion cycle [15].

2.3.2. Symmetry Index Between Hemibody Parts (SI)

The symmetry index (SI, typically called the Robinson Index) measures the relative asymmetry between sides (left-right) for a variable X (stance and airtime, period, forces). It is defined as:

$$SI(X) = \frac{2 * |XL - XR|}{(XL + XR)} 100\% \tag{10}$$

In this form, SI = 0% indicates perfect symmetry; higher values reflect greater asymmetry. It is common in the literature to explicitly use the symmetry index to verify symmetry in different gait signals, thereby validating its use as a standard metric [16].

2.4. A Brief Review of Works

The half-center oscillator (HCO) is the basis of the CPG, which consists of two neurons or two neural populations connected by excitatory and inhibitory neurotransmitters, it checks for possible periodic, quasiperiodic and chaotic rhythms emerging, including self-symmetric and mutually symmetric patterns, using tools such as bifurcations, Poincaré maps, frequency spectra, and routes to chaos [17]. In ref. [18], they built a complete CPG based on delayed Van der Pol oscillators to control a snake-like robot with pitch-yaw configuration.

It uses the spatio-temporal dynamics of coupled oscillators to form a unified CPG control framework capable of generating multiple locomotion patterns in metameric robots using Hopf-type coupled oscillators and versatile coupling laws [19].

Based on delay-coupled Van der Pol oscillators, a system is proposed that generates rhythms with distinct spatiotemporal patterns, thereby providing several types of quadrupedal locomotion [20].

In ref. [21], they show the design, simulation, and prototype of a quadruped robot inspired by cheetah biomechanics, employing Wilson–Cowan neural oscillators to reproduce highly efficient locomotion patterns (trot, pace, gallop).

In ref. [22], they integrate a bioinspired CPG (obtained from a rational mathematical model) with a fuzzy control system to achieve stable and adaptive locomotion in a quadruped robot developed in Gazebo-ROS.

A hybrid MPIC (model predictive impedance control) controller for quadrupeds was developed in [23] that can simultaneously integrate compliant behavior (impedance control) and explicit modeling of contact forces (GRF) using MPC, achieving high-speed locomotion with robust stability against lateral disturbances.

3. Results

3.1. Model Proposed

To start the development of the central pattern generator (CPG), Rand, Cohen, and Holmes' proposals, with their systems of first-order differential equations for two and four neurons (Equations (1)–(6)), were used [12]. Each neuron's response is the reproduction of cyclic signals (oscillators). This scheme is modified to constitute differential equations with an independent term formed by the feedback variable (s). The simulation of equation systems shows transient signals that stabilize over time for any value assigned to the equation system's parameters.

Therefore, the independent linear term of the equations changes by terms of order two and order four. The first two systems of equations of two and four oscillating neurons formed are in [24]. Subsequently, it proposed a set of first-order oscillatory differential equation systems from [25]. It extrapolated for 3, 5, and 6 neurons corresponding to

equations published in [26] for the modulation of oscillatory signals. In this process, the independent component of the equations formed by the feedback variable develops different structures. Additionally, in ref. [26], a neuro-fuzzy evolutionary algorithm was proposed to obtain the appropriate values of the parameters of the differential equation systems to operate as an oscillatory signal or as a transient signal. This algorithm begins by generating one hundred systems of differential equations, randomly assigning parameter values. The fast Fourier transform is used as the performance function to verify the system's periodicity. In fifty percent of cases of poor performance, mutation is applied, randomly modifying half of the parameters. This process is repeated for one hundred iterations to finally select the system of equations with the best performance. Consequently, to find the values of the parameters of the systems of equations of this article, apply the algorithm analyzed in [26].

Although the equations are functional in terms of their initial purpose of generating oscillatory signals, the drawback is lack of uniformity in the conformation of the different systems of equations. Therefore, it proceeds to reformulate the independent term as non-linear with fractional expressions (rationals) formed by the feedback variables in powers of order two that present a specific pattern in their conformation. These systems exhibit cyclical behavior in the signals of each neuron (Equations (11)–(30)) for certain parameter values defined in the equations (Table 1).

Table 1. Definitive first-order differential equation systems.

Parameter	System Two Equations	System Three Equations	System Four Equations	System Five Equations	System Six Equations
A	7.0524	8.6675	5.4020	5.0866	7.2716
B	9.1641	6.3119	0.3027	6.0330	7.3934×10^{-4}
C	6.9250	3.5507	6.9631	1.6140	4.6329
D	6.7999	9.9700	5.1972	6.3545	3.6185
k_1	2.7210	2.2417	0.5903	8.4394	9.5207
k_2	-	6.5245	8.9004	7.8227	9.3219
τ_1	4.3471	6.0499	3.3020	2.6457	2.0654
τ_2	3.9141	3.8725	2.2970	3.1470	1.5970
τ_3	-	1.4219	1.1395	1.8320	5.7176
τ_4	-	-	3.1092	4.4747	5.9292
τ_5	-	-	-	3.2668	6.9861
τ_6	-	-	-	-	3.0581

System of two first-order differential equations:

$$\tau_1 \frac{dy_1}{dt} = -y_1 + \frac{A(k_1 - Dy_2)^2}{(k_1 + Dy_2)^2 + (k_1 - Dy_1)^2} \tag{11}$$

$$\tau_2 \frac{dy_2}{dt} = -y_2 + \frac{A(B - Cy_1)^2}{(B + Cy_1)^2 + (B - Cy_2)^2} \tag{12}$$

System of three first-order differential equations:

$$\tau_1 \frac{dy_1}{dt} = -y_1 + \frac{A(k_1 - Dy_2)^2}{(k_1 + Dy_2)^2 + (k_1 - Dy_1)^2} \tag{13}$$

$$\tau_2 \frac{dy_2}{dt} = -y_2 + \frac{A(k_2 - Dy_1)^2}{(k_2 + Dy_2)^2 + (k_2 - Dy_3)^2} \tag{14}$$

$$\tau_3 \frac{dy_3}{dt} = -y_3 + \frac{A(B - Cy_2)^2}{(B + Cy_2)^2 + (B - Cy_3)^2} \tag{15}$$

System of four first-order differential equations:

$$\tau_1 \frac{dy_1}{dt} = -y_1 + \frac{A(k_1 - Dy_2)^2}{(k_1 + Dy_2)^2 + (k_1 - Dy_1)^2} \tag{16}$$

$$\tau_2 \frac{dy_2}{dt} = -y_2 + \frac{A(k_2 - Dy_1)^2}{(k_2 + Dy_2)^2 + (k_2 - Dy_3)^2} \tag{17}$$

$$\tau_3 \frac{dy_3}{dt} = -y_3 + \frac{A(k_2 - Dy_2)^2}{(k_2 + Dy_3)^2 + (k_2 - Dy_4)^2} \tag{18}$$

$$\tau_4 \frac{dy_4}{dt} = -y_4 + \frac{A(B - Cy_3)^2}{(B + Cy_3)^2 + (B - Cy_4)^2} \tag{19}$$

System of five first-order differential equations:

$$\tau_1 \frac{dy_1}{dt} = -y_1 + \frac{A(k_1 - Dy_2)^2}{(k_1 + Dy_2)^2 + (k_1 - Dy_1)^2} \tag{20}$$

$$\tau_2 \frac{dy_2}{dt} = -y_2 + \frac{A(k_2 - Dy_1)^2}{(k_2 + Dy_2)^2 + (k_2 - Dy_3)^2} \tag{21}$$

$$\tau_3 \frac{dy_3}{dt} = -y_3 + \frac{A(k_2 - Dy_2)^2}{(k_2 + Dy_3)^2 + (k_2 - Dy_4)^2} \tag{22}$$

$$\tau_4 \frac{dy_4}{dt} = -y_4 + \frac{A(k_2 - Dy_3)^2}{(k_2 + Dy_4)^2 + (k_2 - Dy_5)^2} \tag{23}$$

$$\tau_5 \frac{dy_5}{dt} = -y_5 + \frac{A(B - Cy_4)^2}{(B + Cy_4)^2 + (B - Cy_5)^2} \tag{24}$$

System of six first-order differential equations:

$$\tau_1 \frac{dy_1}{dt} = -y_1 + \frac{A(k_1 - Dy_2)^2}{(k_1 + Dy_2)^2 + (k_1 - Dy_1)^2} \tag{25}$$

$$\tau_2 \frac{dy_2}{dt} = -y_2 + \frac{A(k_2 - Dy_1)^2}{(k_2 + Dy_2)^2 + (k_2 - Dy_3)^2} \tag{26}$$

$$\tau_3 \frac{dy_3}{dt} = -y_3 + \frac{A(k_2 - Dy_2)^2}{(k_2 + Dy_3)^2 + (k_2 - Dy_4)^2} \tag{27}$$

$$\tau_4 \frac{dy_4}{dt} = -y_4 + \frac{A(k_2 - Dy_3)^2}{(k_2 + Dy_4)^2 + (k_2 - Dy_5)^2} \tag{28}$$

$$\tau_5 \frac{dy_5}{dt} = -y_5 + \frac{A(k_2 - Dy_4)^2}{(k_2 + Dy_5)^2 + (k_2 - Dy_6)^2} \tag{29}$$

$$\tau_6 \frac{dy_6}{dt} = -y_6 + \frac{A(B - Cy_5)^2}{(B + Cy_5)^2 + (B - Cy_6)^2} \tag{30}$$

The terms or parameters of Equations (11)–(30) are as follows:
τ_i is the time constant variable;

A is global gain;
B is the term of bias;
k_1, k_2 are excitatory base inputs;
C is the sensitivity of the denominator;
D is the coupling between variables.

After verifying the oscillatory behavior of the set of equation systems, it is the ideal tool for implementing the central pattern generators in robotic systems with quadruped legs. Consequently, the general model is below.

$\forall\, i \in \mathbb{Z};\ A, B, C, D, k_1, k_2, \tau_i \in \mathbb{R}$

$i = 1$

$$\tau_i * dy_i/dt = -y_i + \frac{A(k_1 - D * y_{i+1})^2}{(k_1 + D * y_{i+1})^2 + (k_1 - D * y_i)^2} \tag{31}$$

$1 < i < n$

$$\tau_i * dy_i/dt = -y_i + \frac{A(k_2 - D * y_{i-1})^2}{(k_2 + D * y_{i+1})^2 + (k_2 - D * y_i)^2} \tag{32}$$

$i = n$

$$\tau_i * dy_i/dt = -y_i + \frac{A(B - C * y_{n-1})^2}{(B + C * y_n)^2 + (B - C * y_{n-1})^2} \tag{33}$$

The model presented by Equations (31)–(33) corresponds to the generic structure of a system of equations. Equation (31) allows the creation of the mathematical expression of the first neuron with its connections to the rest of the neurons. In Equation (32), the equations correspond to the neurons that are neither the first nor the last, with their respective neuronal connections expressed, with Equation (33) corresponding to the last neuron and its connections with the rest of the neurons mathematically. Consider, for the case of a robotic arm with six degrees of freedom, an oscillating system of six neurons that can configure with a system of six first-order differential equations from the general model, with i between 1 and 6. For the first neuron, $i = 1$, Equation (31) obtains the first differential equation.

$i = 1\ \tau_1 * dy_1/dt = -y_1 + \frac{A(k_1 - D*y_2)^2}{(k_1 + D*y_2)^2 + (k_1 - D*y_1)^2}$

With i between 2 and 5, the following four equations are obtained using Equation (32) like this.

$i = 2\ \tau_2 * dy_2/dt = -y_2 + \frac{A(k_2 - D*y_1)^2}{(k_2 + D*y_3)^2 + (k_2 - D*y_2)^2}$

$i = 3\ \tau_3 * dy_3/dt = -y_3 + \frac{A(k_2 - D*y_2)^2}{(k_2 + D*y_4)^2 + (k_2 - D*y_3)^2}$

$i = 4\ \tau_4 * dy_4/dt = -y_4 + \frac{A(k_2 - D*y_3)^2}{(k_2 + D*y_5)^2 + (k_2 - D*y_4)^2}$

$i = 5\ \tau_5 * dy_5/dt = -y_5 + \frac{A(k_2 - D*y_4)^2}{(k_2 + D*y_6)^2 + (k_2 - D*y_5)^2}$

Finally, the conformation of the last Equation (33) applies with $i = 6$, that is, the nth neuron.

$i = 6\ \tau_6 * dy_6/dt = -y_6 + \frac{A(B - C*y_5)^2}{(B + C*y_6)^2 + (B - C*y_5)^2}$

For the reproduction of cyclical signals, a search and optimization technique must be used to determine the values of the parameters [26], which in the present case are: $A = 9.8834$, $B = 4.0989$, $C = 3.7119$, $D = 2.2685$, $k_1 = 4.4603$, $k_2 = 2.6622$, $\tau_1 = 4.5910$, $\tau_2 = 4.3291$, $\tau_3 = 2.5962$, $\tau_4 = 1.3371$, $\tau_5 = 4.1923$, $\tau_6 = 5.0686$.

3.2. Experimental Verification of the Proposed Method

Next, two cases of quadruped robots are presented. The general model of sets of oscillatory differential equations was used to assemble the central pattern generators in locomotion control.

The systems of differential equations obtained from the model (31)–(33) for its application in quadruped robots corresponds to a system of two Equations (11) and (12), a system of three Equations (13)–(15), and a system of four Equations (16)–(19) that build oscillatory or transitory signals according to the behavior required in each of the levels of locomotion control structure, which the type of signal achieves according to the values assigned to the parameters (A, B, C, D, k_1, k_2, τ_1, τ_2, τ_3, τ_4).

This study analyzes the behavior of previously presented systems of first-order differential equations and uses chaos and bifurcation theory in dynamical systems. Therefore, the procedures employed are time history, bifurcation diagrams, phase diagrams, Poincaré maps, frequency spectrum analysis, and the Lyapunov maximum exponent. The combination of these methods allows us to verify the stability of dynamical systems. The histogram is the basis for the other procedures. Therefore, the following considerations are taken into account when developing the graph: The differential equations are transformed into discrete equations and solved using Euler's method; the initial value for the variables (y_i) is zero; the number of iterations (n) is 200; and the step size (h) is 1. This graph contrasts discrete time (iterations) with each of the output variables (y_i), allowing us to visualize periodicity. The other tools are constructed using the previously collected information. In the case of the phase diagram, the output variables (y_i) are compared to determine the projection of the attractor in the state space. In the frequency spectrum, the fast Fourier transform is calculated to determine dominant and harmonic frequencies. In the Poincaré map, for each variable y_i, a sample of 2π data is taken and compared in two- or three-dimensional graphs to formally validate the periodicity. In the bifurcation diagram, the chosen parameter is A because its influence on the equations lies in being decisive in the amplitude of the signal (gain), and any change can generate drastic changes in the waveform. A is varied between -50 and 50; essentially, it maps the space of parameter A as a function of the output variables (y_i). The maximum Lyapunov exponent allows quantifying sensitivity to initial conditions. Starting from two infinitely close trajectories on the order of 1×10^{-8} and varying parameter A between -50 and 50, an attempt is made to interpret the possible dynamic regimes of the system based on the Chaos Criterion (exponential divergence criterion).

The procedure starts with the system of four equations, with outputs y_1, y_2, y_3, and y_4 (Figures 3–6), with the parameter values from Table 1.

Figure 3A, the time history, shows a transient at the beginning (first few 20 seconds/iterations), followed by a sustained oscillation. The four signals exhibit distinct amplitudes and offsets (they do not oscillate around 0, but rather around a positive level), which is typical of oscillators with saturation. Coordination (consistent phase relationship) is observed between y_1, y_2, y_3, and y_4. Figure 3B (3D phase diagram) shows the initial polygonal section that corresponds to the initial transient of the variables and then concentrates in a closed orbit or a thin band. It demonstrates that the system has a one-dimensional periodic attractor (limit cycle) embedded in a 4-dimensional space; the 3D graph shows its projection onto (y_2, y_3, y_4). It can also be interpreted that the coordination between y_2, y_3, and y_4 is stable and repeatable. This supports the idea that the running pattern for generating CPGs from four oscillators will have time coherence.

Figure 4A shows a large initial polygonal section; this is the transient, where the system travels from the initial conditions to the attractor. In Figure 4B, the frequency spectrum shows a dominant peak (fundamental frequency at 0.23), accompanied by secondary peaks (0.16, 0.26, 0.36, 0.46), but without a dominant broadband (no appearance of chaos).

Figure 5A, the Poincaré map (sampled points every 2π), shows points that follow an organized structure (curved trend), not a scattered cloud. What we see is much more compatible with quasi-periodicity or a high-period periodic oscillation than with chaos.

Meanwhile, in Figure 5B–E, a single continuous band appears in each of the four graphs, almost linear as a function of A. This band is slightly wider in the intermediate zone of A [2, 18]; this width represents the range of values that each output (y_i) takes within the limit cycle.

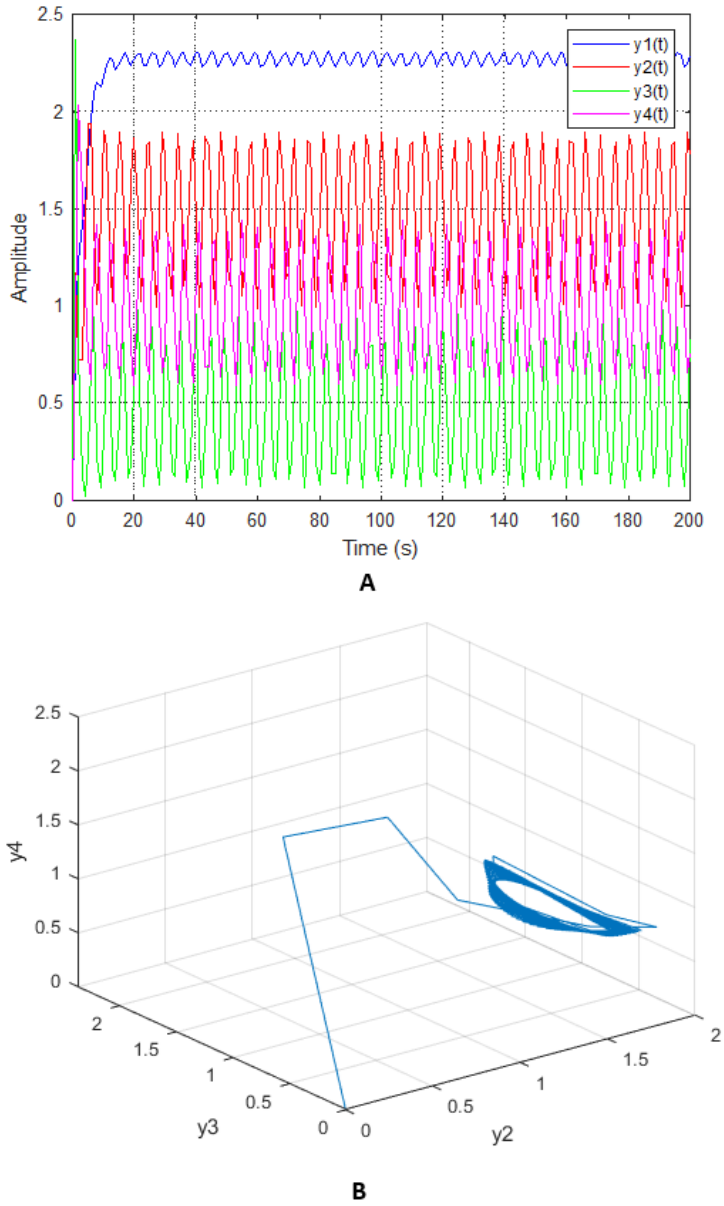

Figure 3. Bifurcation and chaos analysis for parameter A in terms of its outputs y_1, y_2, y_3, y_4. (**A**) Time history. (**B**) 3D phase diagram (y_2, y_3, y_4).

Figure 6 shows a horizontal plateau around λ_{max} in -0.36 for A < 2 and A > 19. An intermediate zone of A ∈ [2, 20] where λ_{max} oscillates between small negative values, zero, and small positive values. The value A is equivalent to 5.4020, which clearly falls in this intermediate zone (critical region), not on the stable plateaus. In this case, the points are very close to the line λ_{max} equal to 0 and $\lambda_{max} < 0$, since the clearly positive peaks are concentrated more towards A ∈ [12, 18].

For A = 5.4020 with $\lambda_{max} = 0.0000495$, the observed behavior is stable and highly structured oscillatory, which means that the system is very close to a transition (stability edge). This is corroborated in the bifurcation diagram, but it is not in the strong zone of

chaos; if chaos exists, it would be very weak in that case. All of the above is supported in the phase diagram and in the frequency spectrum.

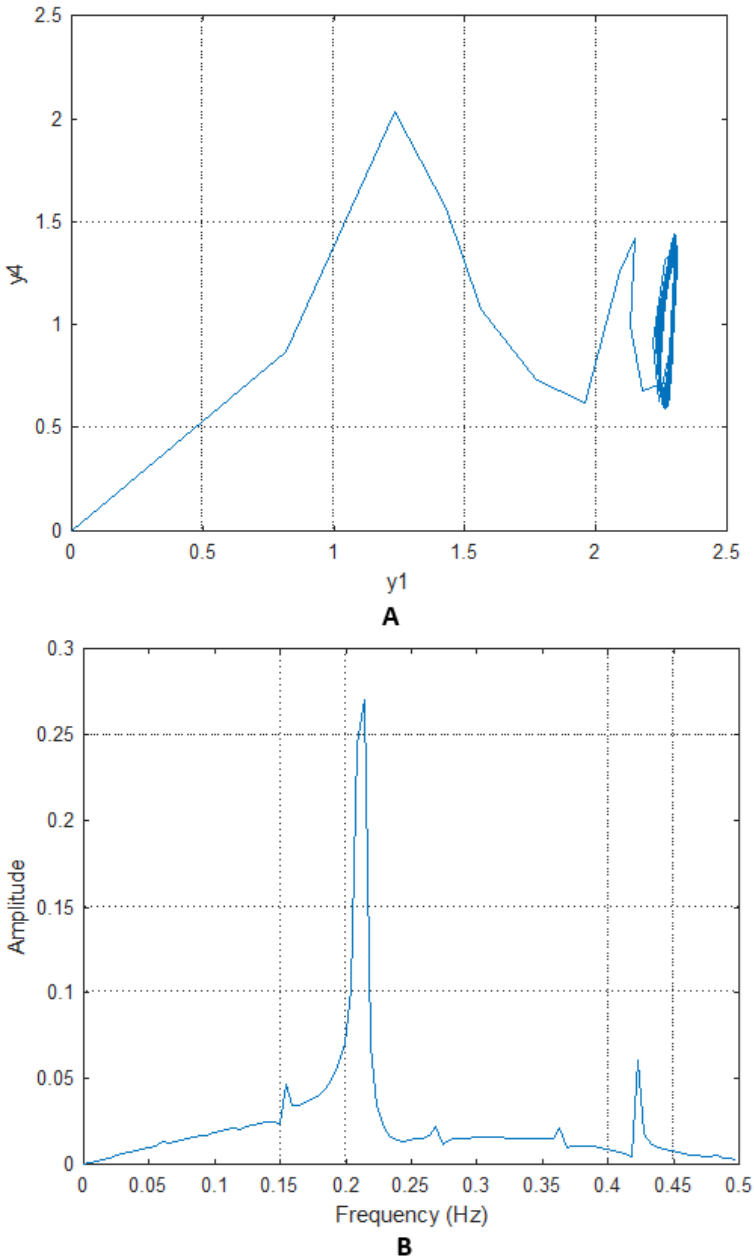

Figure 4. Bifurcation and chaos analysis for parameter A in terms of its outputs y_1, y_2, y_3, y_4. (**A**) Phase plane of y_1,y_4. (**B**) Frequency spectrum.

The answer to the system of three differential equations to the previously established procedures is presented below (Figures 7–10) with the parameter values from Table 1.

In Figure 7A, the three signals exhibit a transient in the first 10 to 20 s, where the amplitudes change rapidly. From then on, all three enter a clearly periodic steady state, but with phase and amplitude differences between them. Regarding Figure 7B, the system has a periodic attractor of dimension 1 (limit cycle) embedded in a space of dimension 3. It is important to note that the repeatability of the orbit indicates high stability. This behavior means that, for locomotion, the three-equation CPG generates a stable coordination pattern among three "modules," which is relevant for repetitive walking rhythms.

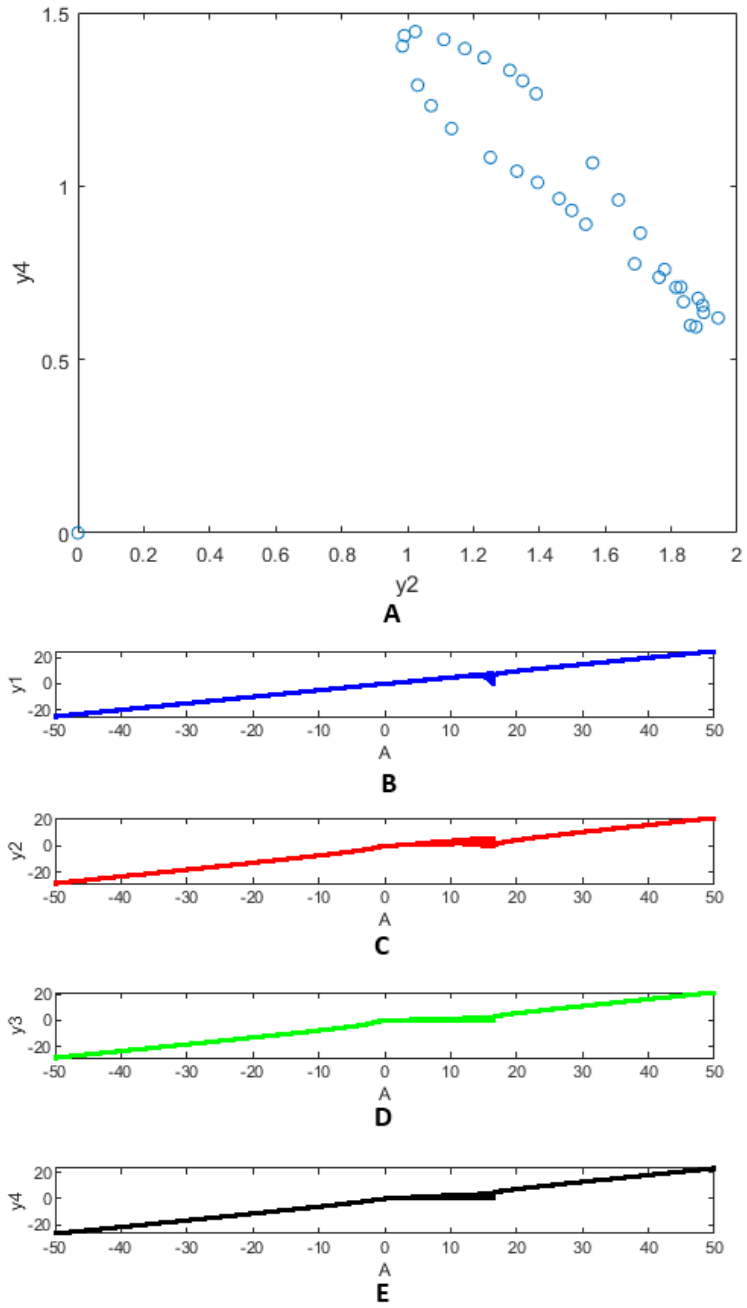

Figure 5. Bifurcation and chaos analysis for parameter A in terms of its outputs y_1, y_2, y_3, y_4. (**A**) Poincaré map. (**B**) Bifurcation Diagram A vs. y_1. (**C**) Bifurcation Diagram A vs. y_2. (**D**) Bifurcation Diagram A vs. y_3. (**E**) Bifurcation Diagram A vs. y_4.

Figure 8A shows a very pronounced dominant peak around 0.16–0.17 Hz and a second harmonic near 0.33–0.35 Hz. Neither an energy continuum nor a fractal frequency structure is observed. In contrast, Figure 8B shows well-ordered points, describing almost an inclined ellipse; they are not dispersed in space. Therefore, the appearance of a thin, structured cloud, rather than a thick ring, confirms that the system is low-period periodic, not quasi-periodic or chaotic.

Figure 9A–C show a single main band of points that grows approximately linearly with parameter A (from −50 to 50). There is a slightly thickened "band" around a certain interval of A [0, 18], corresponding to the range of values that each y_i takes within the limit cycle. No period doubling, multiple branches, or scattered point clouds are observed. This aspect of CPG development means that you can modulate A to adjust the amplitude

and/or offset of the pattern as a function of step height or joint range without risking entering chaotic or multistable regimes, since the pattern remains well-defined.

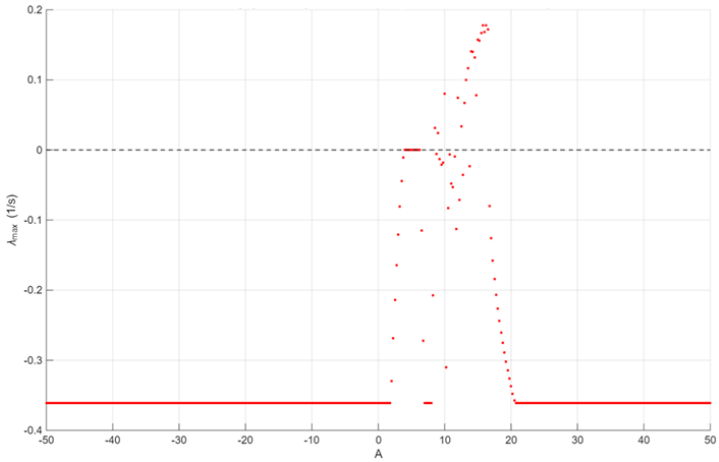

Figure 6. Bifurcation and chaos analysis for parameter A in terms of Lyapunov maximum exponent (y_1, y_2, y_3, y_4)

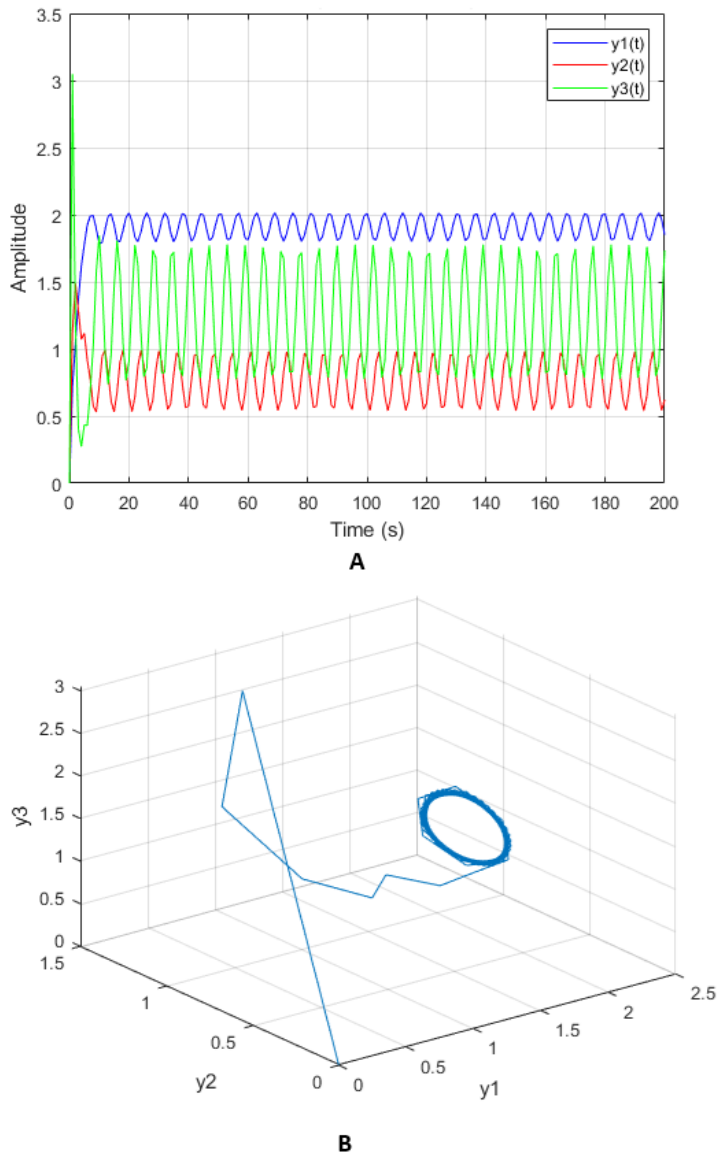

Figure 7. Bifurcation and chaos analysis for parameter A in terms of its outputs y_1, y_2, y_3. (**A**) Time history. (**B**) 3D phase diagram (y_1, y_2, y_3).

The diagram in Figure 10 shows three clearly differentiated dynamic regions: the interval of A in [−50, 0] and [18, 50] with λ_{max} close to −0.18 (constant and negative), the transition region A ∈ [0, 18] where λ_{max} crosses negative values and approaches zero in the interval [0, 15] and has positive peaks in the interval [15, 18]. In the graphs of the maximum Lyapunov exponent and the bifurcations of the output variables, a consistency exists in that the changes arise in the interval A [0, 18], where as in A = 8.6675 with λ_{max} = 0.0000495, the discretized system of three equations is in a marginally stable regime, close to a bifurcation, compatible with high period periodicity or quasi-periodicity, without real conclusive evidence of sustained chaos, as observed in the frequency spectrum.

The behavior of the system of two differential equations when applying procedures in the time and frequency domain is presented below (Figures 11–14) with the parameter values from Table 1.

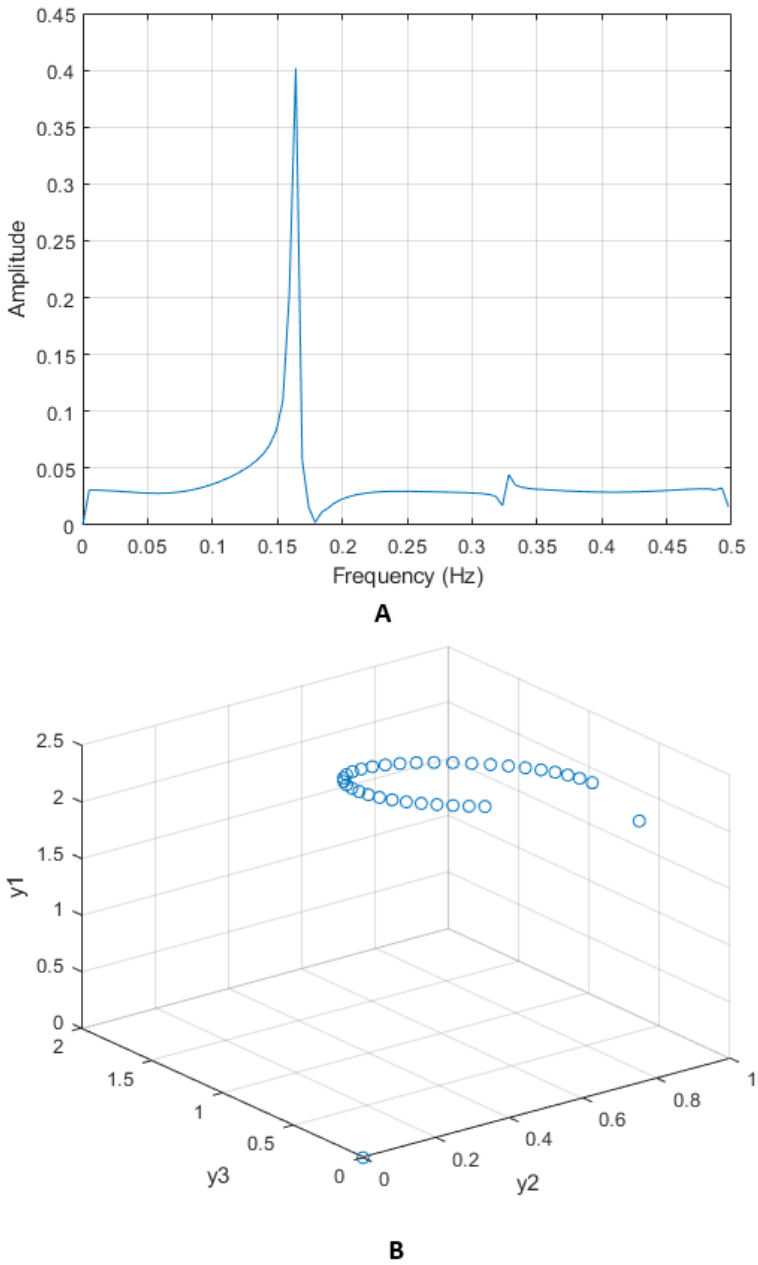

Figure 8. Bifurcation and chaos analysis for parameter A in terms of its outputs y_1, y_2, y_3. (**A**) Frequency spectrum. (**B**) Poincaré map.

In Figure 11A, regular and persistent oscillations are observed, with y_1 and y_2 coupled and exhibiting a relatively consistent phase shift. The amplitude appears bounded and stationary after the transient, providing evidence of a periodic attractor. Meanwhile, Figure 11B presents a closed trajectory of the deformed ellipse type (with the typical "mesh" or repeated trace), which is consistent with a limit cycle (periodic attractor), without chaos (which would give a filled region and not a closed repetitive curve).

Figure 12A shows a dominant peak around 0.12–0.13 Hz, with harmonics at 0.25 Hz and 0.37 Hz. Furthermore, there is no broadband noise or a continuum of significant frequencies. In Figure 12B, instead of a single point, a discrete set of a few points is observed on a closed curve. These points are ordered and well-structured, not filling a dense region, indicating a periodic or finite-period, non-chaotic orbit.

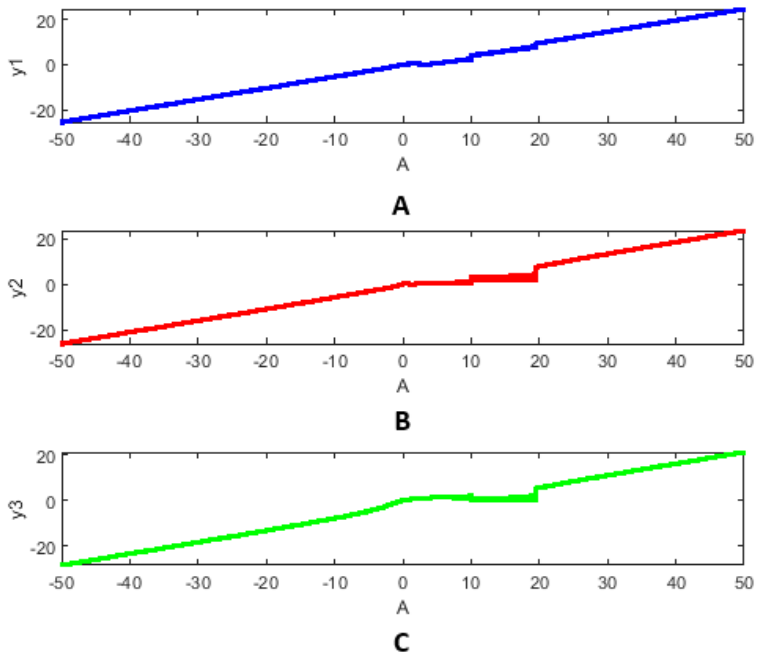

Figure 9. Bifurcation and chaos analysis for parameter A in terms of its outputs y_1, y_2, y_3. (**A**) Bifurcation Diagram A vs. y_1. (**B**) Bifurcation Diagram A vs. y_2. (**C**) Bifurcation Diagram A vs. y_3.

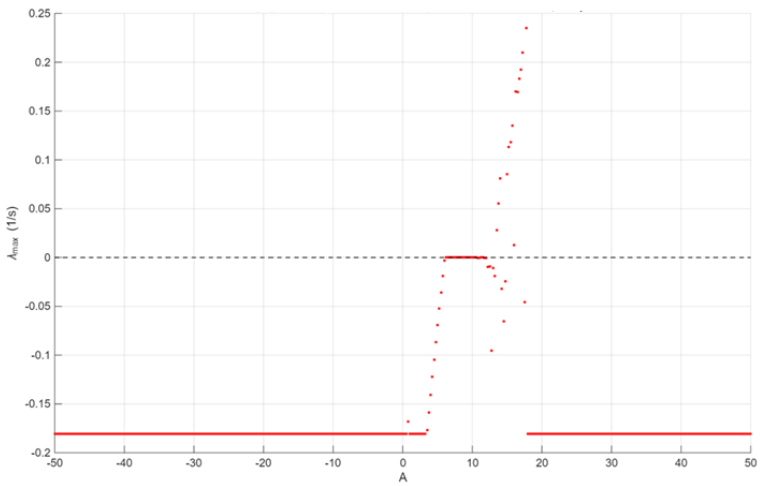

Figure 10. Bifurcation and chaos analysis for parameter A in terms of Lyapunov maximum exponent (y_1, y_2, y_3).

In Figure 13A,B, a single, almost linear branch appears across the entire range of A. No branching, multiple bands, or point clouds typical of chaos are observed. This indicates that, for each value of A, the system converges to a single stable regime. However, in the interval of A [0, 15], a slight thickening of the curve is seen (several points very close together), which corresponds to the amplitude of the limit cycle. Consequently, if A is one of the CPG design parameters for managing gain, bias, or coupling component to determine the running mode, it is viable since a parameter range is being chosen in which the CPG produces a well-defined and robust running pattern.

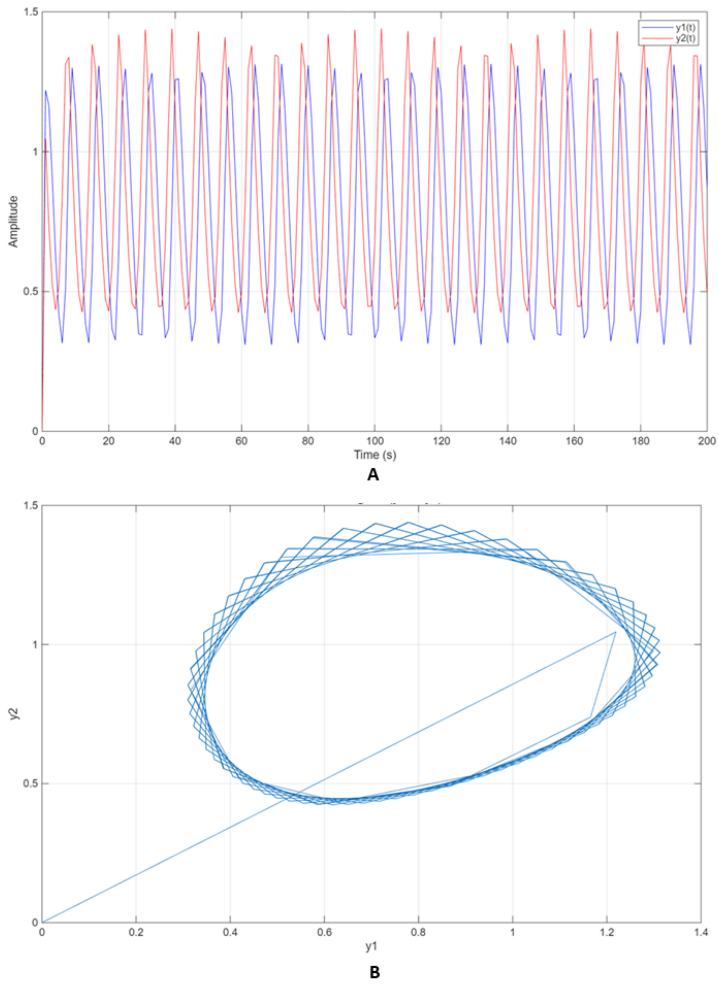

Figure 11. Bifurcation and chaos analysis for parameter A in terms of its outputs y_1, y_2. (**A**) Time history. (**B**) Phase diagram (y_1, y_2).

Figure 14 shows three regions: A < 0 with λ_{max} tending to -0.45, A > 15 with λ_{max} tending to -0.4, and a critical zone around A $\in$ [0, 15]: scattered points approaching 0, with some positive peaks and oscillations.

For A = 7.0524 with $\lambda_{max} = -0.00189$, the system operates in a stable periodic window, very close to the threshold (because λ_{max} is close to zero). In terms of CPG-type locomotion, this is desirable for a repeatable, stable pattern with the possibility of fine transitions as A varies.

These systems of two, three, and four first-order differential equations used such as oscillatory signals (Figures 5A, 8A and 11A) in [27] for dog-type robot (Figure 15A) and in [22] for crab-type robot (Figure 15B) built from the new model reinforces the previously carried out analysis of its viability aplication such as CPG for locomotion. The graphs obtained from values assigned to the parameters A, B, C, D, k_1, k_2, τ_1, τ_2, τ_3, τ_4 of Table 1.

The parameter values are defined using the neuro-fuzzy evolutionary algorithm exposed in [26].

According to [22], the behavior of the crab-type robot in its locomotion is shown in the simulation in Gazebo–ROS in its Slow, Normal and Fast Advance movements. The general aspects of the robot's locomotion in its three types of locomotion are presented in Table 2. Aspects as the movement synchronization of each leg and the coordination of movements of all four legs. These specific movements are executed during the locomotion cycle in a time between 1 and 6 s.

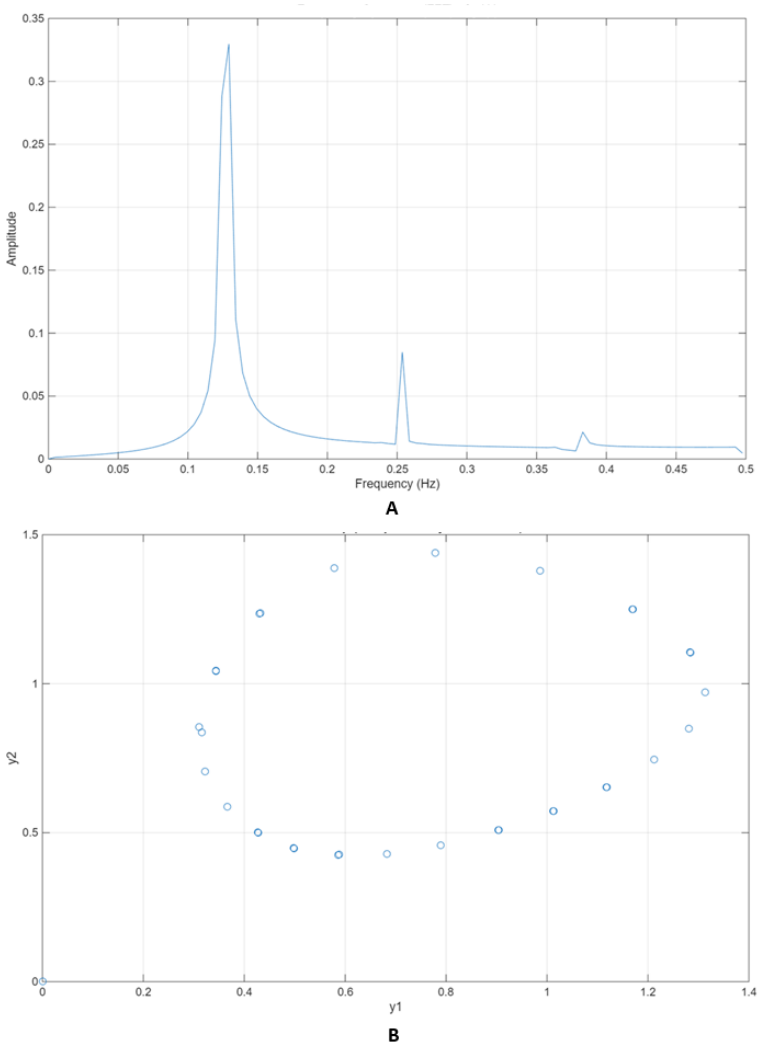

Figure 12. Bifurcation and chaos analysis for parameter A in terms of its outputs y_1, y_2. (**A**) Frequency spectrum. (**B**) Poincaré map.

The characteristics arising in the transition between the types of locomotion are seen in Table 3. It can be observed that the transition between slow advance, normal advance, and fast advance locomotion of a crab quadruped robot in static equilibrium or quasi-static possesses a response capacity (according to operating frequency) in the worst case, about 1.3 s, versus a possible rollover.

According to [27], the behavior of the dog-type robot in its locomotion of a real R4A3 prototype is shown in its walk and trot movements. The general aspects of the robot's locomotion in its two types of locomotion are presented in Table 4. Aspects as the movement synchronization of each leg and the coordination of movements of all four legs. These specific movements are executed during the locomotion cycle in a time between 0.5 and 4 s.

The characteristics arising in the transition between the types of locomotion are seen in Table 5. It can be observed that the transition between walk and trot locomotion of a crab quadruped robot in static equilibrium or quasi-static possesses a response capacity (according to operating frequency) in the worst case, about 1 s, versus a possible rollover.

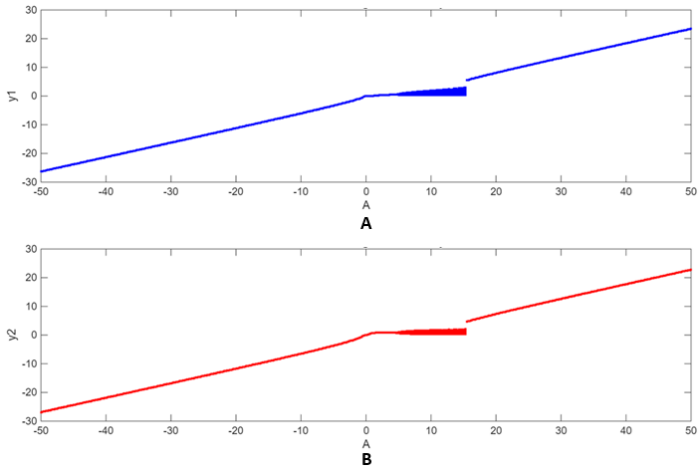

Figure 13. Bifurcation and chaos analysis for parameter A in terms of its outputs y_1, y_2. (**A**) Bifurcation Diagram A vs. y_1. (**B**) Bifurcation Diagram A vs. y_2.

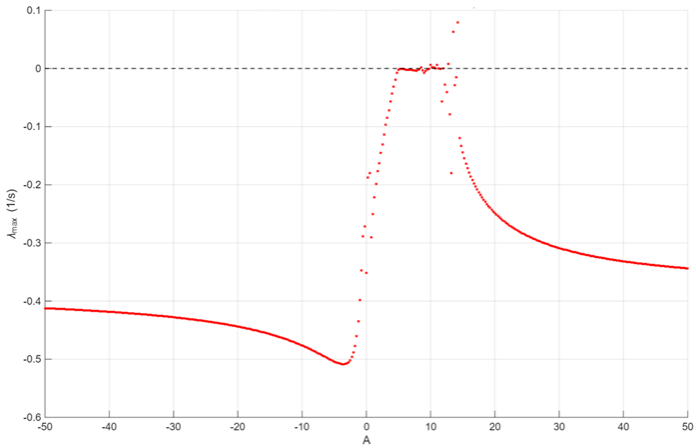

Figure 14. Bifurcation and chaos analysis for parameter A in terms of Lyapunov maximum exponent (y_1, y_2).

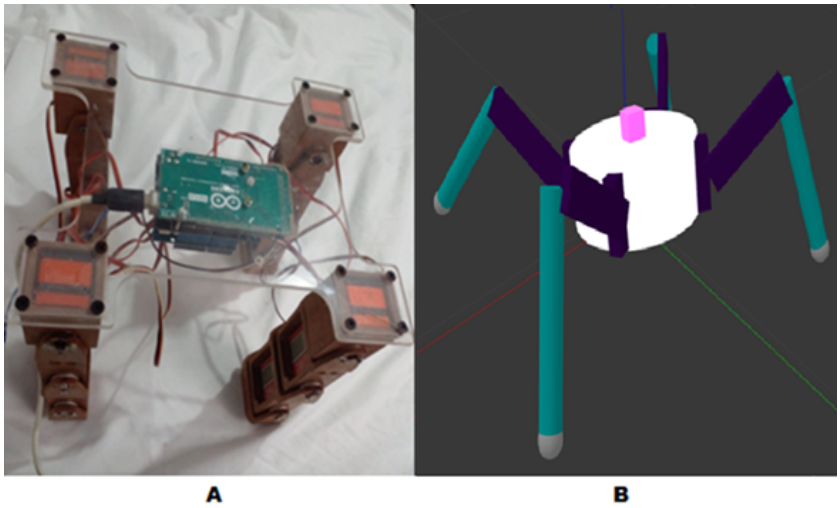

Figure 15. Quadruped robots: (**A**) Dog type. (**B**) Crab type.

Table 2. Types of locomotion of robot crab.

Characteristics	Slow Advance	Normal Advance	Fast Advance
Frequency of locomotion operation	0.15 Hz	0.22 Hz	1.66 Hz
Frequency of operation of each leg in locomotion	0.62 Hz	1 Hz	3.33 Hz
Locomotion sequence	The front legs move, and then alternately move	The right legs initiate the movement, followed by the left legs; each leg at a time	The front legs move at the same time, and then the hind legs move at the same time
Time in support phase per left leg	5.45 s	4.02 s	0.41 s
Time Air phase per left leg	0.81 s	0.49 s	0.189 s
Time in support phase per right leg	5.61 s	4.1 s	0.39 s
Time Air phase per right leg	0.787 s	0.508 s	0.206 s
Joint 1 Angle Range	$[-90°, 90°]$	$[-90°, 90°]$	$[-90°, 90°]$
Joint 2 Angle Range	$[-45°, 45°]$	$[-45°, 45°]$	$[-45°, 45°]$
Joint 3 Angle Range	$[-45°, 45°]$	$[-45°, 45°]$	$[-45°, 45°]$

Table 3. Transition between the types of locomotion of robot crab.

Characteristics	Observation of Slow—Normal Advance	Observation of Normal—Fast Advance	Observation of Fast—Slow Advance
Frequency used	0.62–1 Hz	1–3.33 Hz	3.33–0.62 Hz
Specific leg movements	The locomotion transition occurs at the end of cycle	The locomotion transition occurs at the end of cycle	The locomotion transition occurs at the end of cycle
Rollover situations	N/A	N/A	N/A
Time in support phase per left leg	5.45–4.02 s	4.02–0.41 s	0.41–5.45 s
Time in Air phase per left leg	0.81–0.49 s	0.49–0.189 s	0.189–0.81 s
Time in support phase per right leg	5.61–4.1 s	4.1–0.39 s	0.39–5.61 s
Air phase time per right leg	0.787–0.508 s	0.508–0.062 s	0.206–0.787 s

Considering the data obtained from the locomotion of both the dog robot and the crab robot, comparable metrics such as support factor (β) and symmetry index between

hemibody parts (SI) are presented in Table 6 to quantify qualitative aspects related to the types of balance and transitions that the robots developed in locomotion.

Table 4. Types of locomotion of robot dog.

Characteristics	Walk	Trot
Frequency of locomotion operation	1 Hz	4 Hz
Frequency of operation of each leg in locomotion	0.25 Hz	2 Hz
Locomotion sequence	One leg at a time in the aerial phase	Alternate front–rear legs in support or aerial phase
Time in support phase per left leg	3.8 s	0.2 s
Time Air phase per left leg	0.31 s	0.28 s
Time in support phase per right leg	3.7 s	0.19 s
Time Air phase per right leg	0.28 s	0.26 s
Joint 1 Angle Range	[70°, 140°]	[70°, 140°]
Joint 2 Angle Range	[90°, 150°]	[90°, 150°]
Joint 3 Angle Range	[110°, 170°]	[110°, 170°]

Table 5. Transition between the types of locomotion of robot dog.

Characteristics	Observation of Walk—Trot	Observation of Trot—Walk
Frequency used	1–4 Hz	4–1 Hz
Specific leg movements	Immediate change of locomotion	Immediate change of locomotion
Rollover situations	N/A	N/A
Time in support phase per left leg	3.8–0.2 s	0.2–3.8 s
Time Air phase per left leg	0.3–0.28 s	0.28–0.3 s
Time in support phase per right leg	3.7–0.19 s	0.19–0.3.8 s
Time Air phase per right leg	0.22–0.26 s	0.26–0.22 s

Table 6. Metric support factor (β), symmetry index between hemibody parts (SI), and periods (T).

Robot	Gait	β Izq	β Der	β Prom	SI Support	SI Air	SI Period	Period (T)
Crab	Slow	0.871	0.877	0.874	2.89%	2.88%	2.16%	6.26 s
Crab	Normal	0.891	0.890	0.891	1.97%	3.61%	2.15%	4.51 s
Crab	Fast	0.684	0.654	0.669	5.00%	8.61%	0.50%	0.599 s
Dog	Walk	0.927	0.944	0.935	2.67%	10.17%	3.21%	4.11 s
Dog	Trot	0.417	0.422	0.419	5.13%	7.41%	6.45%	0.48 s

4. Discussion

The main findings of the review of works in robotic systems on control techniques and types of locomotion are presented below.

In [17–22], oscillators are used to form central pattern generators that allow the reproduction of motor functions such as locomotion in its different forms and transitions, mostly in known and generally flat environments.

When analyzing the applications of the robot, it can be determined that the works most similar in functionality are [20,23]. They are quadruped robots with two or more joints or elastic joints per leg, and they perform locomotion, taking into account stability in their movement.

Taking into account the above information, we will focus on discussing those works that propose mathematical structures to reproduce oscillators, which are the basis for emulating CPG, from a qualitative analysis.

In references [18,20], three variant structures of the nonlinear Van der Pol oscillator are presented, widely used as the basis of central pattern generators (CPG), whose expressions exhibit the following basic characteristics.

Second-order with nonlinearity in the damping.

Most jobs have an explicit coupling delay [20].

Nonlinear damping term dependent on a quadratic factor.

Self-sustained oscillatory behavior.

A half-center oscillator with explicit delay (DHCO), is proposed in [17]. These are the typical features.

Nonlinear second-order model.

Each variable depends on the other with a time lag.

Can be tuned to produce synchrony, antiphase, or chaotic rhythms depending on f and τ.

Phase control is possible through delay and coupling constants.

Furthermore, in reference [19], there are derivations or extensions of the Hopf oscillator used to reproduce CPG with the following typical characteristics.

They generate stable or synchronized limit orbits.

Most have phase-angle-dependent coupling, which requires trigonometric evaluation.

Suitable for large networks, with variations in the connection form (phase, matrix, or vector functions).

The Wilson–Cowan mathematical model was also found in [21], with the same mathematical structure of first-order systems of ordinary differential equations (ODEs), neuronal population type, with the following characteristics.

Its mathematical configuration allows for reduced computational cost.

The activation function, the hyperbolic tangent, allows for a continuous and differentiable response.

It does not generate autonomous oscillations, but is ideal for systems controlled or stimulated by external input.

It is highly scalable for distributed networks, functional in CPG-type neural network implementations with multiple nodes.

Ref. [22] uses the system of equations obtained from the model proposed in this paper. In Equations (31)–(33), which correspond to a generalized rational model for n nodes, these are the typical characteristics:

It consists of first-order nonlinear differential equations (ODEs).

The network interactions are successive, meaning that each node depends on the node that precedes or follows it.

It is a nonlinear, rationally symmetric system that behaves similarly to smooth activation functions.

According to the analysis using chaos and bifurcation theory, it is generally stable with a minimal tendency toward chaos.

The three systems of differential equations (two-equation system, three-equation system, and four-equation system) were formed from the proposed model.

Based on the above, it can be inferred that:

(1) In terms of processing, the computational cost of the rational model proposed in this article and in the two applications that use this model offers the lowest computational load per node, considering that the coupling between nodes is algebraic. Therefore, this model is relevant for simple real-life robots with basic locomotion, such as walking, crawling, dragging, or smooth transitions between locomotion modes. It is implemented using low-power controllers, such as 8- or 16-bit microcontrollers, Arduino, ESP32, and others. It is not the case with other models, which require complex trigonometric calculations or higher memory consumption because they need to store history and interpolation, thus requiring more powerful processors. In the case of the Van der Pol model, the computationally expensive function is delayed interpolation, as it requires a significant memory footprint. In the case of the Wilson–Cowan model, the tanh function is applied, which implies the use of highly computationally intensive expressions with exponential functions. In the case of the Hopf model and phase oscillators, they have sine and cosine functions, which involve approximate calculations using the Taylor series. In the half-center oscillator, they require greater computation, since their equations are of second order.

(2) If analyzed from the perspective of versatility with respect to scalability for large or distributed systems, the proposed model can be applied to systems with many nodes, such as modular robots or robotic swarms or robots with multiple joints. Its local structure makes it ideal for decentralized implementation, as each node depends on only one or two neighbors, resulting in low coupling and an easy-to-implement distributed system. In contrast, in the Van der Pol model, as the number of nodes increases, the system becomes more rigid and difficult to integrate numerically. In the Wilson–Cowan model, if nodes are densely dependent on each other, one cannot be updated without knowing all the others. In the Hopf model, increasing the number of nodes with different frequencies complicates the stability of the global network. In the half-center oscillator, link multiplication occurs with delay and buffers per connection, making the analysis complex and reducing its adaptation to possible changes.

(3) In terms of analytical simplicity and design, the model proposed in this article has a clear algebraic structure differentiated by start, middle, and end parts. It implies great ease of understanding, adjusting, and deriving analytical properties such as equilibrium or response regions. It is worth noting that the fact that the three systems of differential equations used as CPGs in the two publications [22,27] come from the proposed model demonstrates its versatility and flexibility, considering that systems of up to six differential equations can be present, compared to the different mathematical structures shown in the other papers, which are rigid and fixed. It allows us to conclude that the model is ideal in contexts where mathematical transparency or robustness in the design is required without relying on complex analysis tools, which are fundamental and necessary in other models. In the Van der Pol model, the difference of squares term multiplied by the derivative prevents direct linear analysis. In contrast, the Wilson–Cowan model employs a smooth Tanh function. Still, its derivative depends strongly on μ, which distorts the analysis near the origin. In the Hopf model, the coupling by the rotation matrix between nodes depends on

relative angles, this makes its analysis more complex since it cannot use in Cartesian coordinates but in polar coordinates. In the half-center oscillator, the are differential equations with delay whose future state depends on a complete history, not only on the current state, which requires advanced tools.

Next, we will focus on the discussion from a quantitative analysis of those works that propose similar locomotion applications to verify their behavior based on the support factor and the symmetry index between hemibody parts.

Tables 2–5 describe the gait modes of the crab [22] and dog [27] robots in terms of frequencies, stance times, and air phase, while Table 6 summarizes, for each gait, the mean support factor (β) and the hemibody symmetry indices: SI Support (asymmetry in stance time), SI Air (asymmetry in air phase), SI Period (asymmetry in cycle period), as well as the total period T. In general, the values in Table 6 indicate that: "Static" gaits (Crab Slow and Normal, Dog Walk) exhibit a high β(0.87–0.94) and a low SI Support [2%, 3%]. The "fast" gaits (Crab Fast and Dog Trot) reduce β to 0.67 and 0.42, respectively, with a slightly higher SI Support (approximately 5%), but a still low SI Period (SI Period < 7%).

In ref. [20], a CPG of four delayed-coupled VDP oscillators is proposed to explicitly generate the classic quadruped gaits (lateral-walk sequence, diagonal-walk sequence, trot, pace, bound, pronk). The aim is to map parameter regions (delays and coupling weights) to specific gait types through bifurcation analysis and phase synchronization.

1. Gait Taxonomy in Terms of Phase Relationships:

The article [20] does not explicitly define duty factor ($\beta*$), but classifies gaits according to phase relationships between the four legs (trot has opposing diagonal pairs, pace is characterized by lateral pairs, and bound develops between anterior and posterior pairs).

Crab and dog robots utilize precisely this implicit taxonomy:

- Dog Walk: "one leg at a time in the air phase" with an asymmetric walk-like pattern, high β.
- Dog Trot: "alternating front and rear legs" with a diagonal trot pattern.
- Crab Fast advance: a pattern where the front legs move together, followed by the rear legs, equivalent to a moderate bound.

2. Correspondence with β and T:

In the ref. [20] model, transitioning from walk to trot and bound reduces the time spent in stance and increases the oscillation frequency. This is consistent with the drop in β from 0.93 (dog Walk) to 0.42 (dog Trot) and T from 4.1 s to 0.48 s, in Table 6. Similarly, crab changes β from 0.87 (Slow) to 0.67 (Fast) with a sharp reduction in period (from 6.26 s to 0.60 s), which fits with the expected behavior when moving in the bifurcation diagram (Figure 9) of [20] from a walk region to a running/bound region.

3. Time Symmetry:

In ref. [20], it is stated that identical oscillators and symmetric couplings are used; therefore, the resulting gaits are intrinsically symmetric hemibody. This hypothesis is reflected in crab and dog by:

- Left β is approximately equal to right β (differences less than 0.03 in all cases in Table 6).
- SI support between 2% (crab normal) and 5% (dog trot), values close to the measurable noise in physical systems.

In the work of [23], model predictive impedance control (MPIC) is introduced for quadrupeds, and crucially, an explicit optimization of the duty factor β as a function of speed is formulated.

Definition and meaning of duty factor:

MPIC defines β as the ratio between stance time and gait period.

It is shown that β has two opposing effects:

- A large β means a longer stance and therefore smaller ground reaction forces (GRF).
- A small β means a longer swing and therefore a lower required leg speed in the air.

β Optimization Model:

Using the kinetic energy of the swinging leg and the vertical impulse of the GRF, a minimization problem is formulated, yielding a closed-form solution for the optimal duty factor (Equation (35) of [23]), as a function of v (speed) and α (weight parameter). Quantitatively, ref. [23] presents a graph of duty factor vs. speed in Figure 2, which is interpreted as a curve that duty factor decreases monotonically with increasing speed. According to the article, these values align with experimental measurements in animals. Where at low speeds, the duty factor is large and at high speeds, the duty factor is low.

Locomotion Equivalents:

It is important to note that in [23], when locomotion at high speeds is described in the Crab and Dog robots of this article, it is expressed as fast locomotion or trotting, and in [23], when locomotion at low speeds is described in the crab and dog robots of this article, it refers to slow, normal, or walking locomotion.

Comparison of [23] with crab and dog robots:

In crab and dog robots, slow gaits (Slow/Normal/Walk) have β centred at 0.87 y 0.94, very consistent with the upper band of β predicted by [23] for low speeds, where stability and GRF reduction are prioritized.

For crab fast (β = 0.67, T = 0.60 s) and dog trot (β = 0.42, T = 0.48 s), the values clearly shift towards the low β region, as observed in [23] when speed is high: longer air phase and shorter support time, a necessary condition for running and/or galloping.

In both robots (crab and dog), the SI Support and SI Period symmetry indices remain below 6%, indicating that, even with reduced β, the temporal distribution between hemi-bodies remains almost perfectly bilateral. This aligns with the approach in [23]: the optimal gait not only minimizes GRF and swing energy but also maintains a symmetrical and stable force pattern throughout the locomotion cycle.

5. Conclusions

The movements reproduced through systems of first-order oscillatory differential equations involving two, three, and four neurons enable the emulation of the forward locomotion of two quadruped robots in both static and dynamic equilibrium. The model reproduced in this work is implemented in two quadruped robots (a dog and a crab) with three degrees of freedom per leg for locomotion on a flat surface.

The results shown in Tables 2–5 present operational data for the robots (crab and dog) to which the proposed mathematical model was applied. Tables 2 and 4 show specific data describing the types of equilibrium in which the robots operate. These characteristics include high support phase times and low air phase times for static equilibrium, as well as low air and support phase times for dynamic equilibrium. Tables 3 and 5 present data on the procedure for transitioning between locomotion types, highlighting differences in their application. For example, the crab transition is synchronous, as it occurs at the end of the cycle, while the dog transition is asynchronous; the current cycle is interrupted with an abrupt jump in support time, all of the above is confirmed by the data in Table 6 with the support factor and the symmetry index.

In a judicious comparative study between the publications shown in the review of works, it was found that unlike presented publications by other authors analyzed, the proposed work demonstrates the advantages of a new experimental mathematical model in aspects such as versatility, simplicity, and processing, in addition, chaos and bifurcation

analysis highlights the absence of chaos in specific cases of differential equation systems derived from the unpublished mathematical model.

Regarding the application in robotics systems, among robots with similar functionality, it is observed that in the analysis of locomotion behavior using metrics such as support factor and symmetry index of the Table 6, the applications published from the proposed new model stand out because the data are similar to other works. The data from the crab and dog robots match the values of the duty factor vs. speed curve proposed in [23], this suggests that the patterns implemented in the crab and dog robots are consistent: slow gaits in the high and stable β region, fast gaits in the low β region, but with preserved time symmetry. The model of [20] based on VDP with delays indicates that the gaits of the crab and dog robots are well implemented. The β and SI metrics in the tables indicate that the physical (or simulated) realization of these gaits is consistent with the mathematical ideal: correct phase relationships, high symmetry, transition from high to low β when moving from slow to fast gears.

Author Contributions: Conceptualization, methodology, formal analysis, investigation, writing original draft preparation, writing review and editing, funding acquisition and resources: E.-M.R.-M. and J.-A.H.-R.; software: E.-M.R.-M.; validation: J.-A.H.-R. All authors have read and agreed to the published version of the manuscript.

Funding: This work was funded under a joint project between Universidad Nacional de Colombia and Servicio Nacional de Aprendizaje, Grant 52316.

Data Availability Statement: The original contributions presented in this study are included in the paper. Further inquiries can be directed to the corresponding author.

Conflicts of Interest: The authors declare no conflicts of interest.

References

1. Ginnobili, S.; Blanco, D. Wallace's and Darwin's natural selection theories. *Synthese* **2019**, *196*, 991–1017. [CrossRef]
2. Zenkevich, L.A. The evolution of animal locomotion. *J. Morphol.* **1945**, *77*, 1–52. [CrossRef]
3. Rubio, F.; Valero, F.; Llopis-Albert, C. A review of mobile robots: Concepts, methods, theoretical framework, and applications. *Int. J. Adv. Robot. Syst.* **2019**, *16*, 1729881419839596. [CrossRef]
4. Torres-Pardo, A.; Pinto-Fernández, D.; Garabini, M.; Angelini, F.; Rodriguez-Cianca, D.; Massardi, S.; Tornero, J.; Moreno, J.C.; Torricelli, D. Legged locomotion over irregular terrains: State of the art of human and robot performance. *Bioinspir. Biomim.* **2022**, *17*, 061002. [CrossRef] [PubMed]
5. Ijspeert, A.J.; Crespi, A.; Cabelguen, J.-M. Simulation and Robotics Studies of Salamander Locomotion: Applying Neurobiological Principles to Control Locomotion in Robots. *J. Neuroinform.* **2005**, *3*, 171–195. [CrossRef] [PubMed]
6. Ijspeert, A.J. Central pattern generators for locomotion control in animals and robots: A review. *Neural Netw.* **2008**, *21*, 642–653. [CrossRef] [PubMed]
7. Grillner, S.; Zangger, P. On the Central Generation of Locomotion in the Low Spinal Cat. *Exp. Brain Res.* **1979**, *34*, 241–261. [CrossRef] [PubMed]
8. Marder, E.; Bucher, D. Central pattern generators and the control of rhythmic movements. *Curr. Biol.* **2001**, *23*, R986–R996. [CrossRef] [PubMed]
9. Kassim, M.H.; Zainal, N.H.; Arshad, M.R. Central Pattern Generator in Bio-inspired Robot: Simulation using MATLAB. In Proceedings of the 2nd International Conference Underwater System Technology, Bali, Indonesia, 4 November 2008.
10. Squire, L.; Berg, D.; Bloom, F.; Lac, S.D.; Ghosh, A.; Spitzer, N. *Fundamental Neuroscience*, 3rd ed.; Academic Press: Cambridge, MA, USA, 2008; pp. 1–1280.
11. Pierre, A.G. The mammalian central pattern generator for locomotion. *J. Brain Res. Rev.* **2008**, *62*, 45–56.
12. Crook, S.; Cohen, A. Central Pattern Generators. In *The Book of Genesis*; Bower, J.M., Beeman, D., Eds.; Springer: New York, NY, USA, 1998; pp. 131–147.
13. Kuznetsov, Y.A. *Elements of Applied Bifurcation Theory*, 2nd ed.; Springer: New York, NY, USA, 1998; pp. 1–553.
14. Karaaslanlı, C. Bifurcation Analysis and Its Applications. In *Numerical Simulation—From Theory to Industry*; Andriychuk, M., Ed.; IntechOpen: Rijeka, Croatia, 2012; pp. 1–34.

15. Patoz, A.; Lussiana, T.; Thouvenot, A.; Mourot, L.; Gindre, C. Duty Factor Reflects Lower Limb Kinematics of Running. *J. Appl. Sci.* **2020**, *10*, 8818. [CrossRef]
16. Daniluk, A.; Hadamus, A.; Ludwicki, M.; Zagrodny, B. Backward vs. Forward Gait Symmetry Analysis Based on Plantar Pressure Mapping. *J. Symmetry* **2022**, *14*, 203. [CrossRef]
17. Song, Z.; Xu, J. Self-/mutual-symmetric rhythms and their coexistence in a delayed half-center oscillator of the CPG neural system. *J. Nonlinear Dyn.* **2022**, *108*, 2595–2609. [CrossRef]
18. Song, Z.; Huang, X. ; Xu, J. Spatiotemporal pattern of periodic rhythms in delayed Van der Pol oscillators for the CPG-based locomotion of snake-like robot. *J. Nonlinear Dyn.* **2022**, *110*, 3377–3393. [CrossRef]
19. Zhou, Q.; Xu, J.; Fang, H. A CPG-Based Versatile Control Framework for Metameric Earthworm-Like Robotic Locomotion. *J. Adv. Sci.* **2023**, *10*, 2206336. [CrossRef] [PubMed]
20. Song, Z.; Zhu, J.; Xu, J. Gaits generation of quadruped locomotion for the CPG controller by the delay-coupled VDP oscillators. *J. Nonlinear Dyn.* **2023**, *111*, 18461–18479. [CrossRef]
21. Hernández-Flores, E.A.; Hernández-Rodríguez, Y.M.; Munguía-Fuentes, R.; Bayareh-Mancilla, R.; Cigarroa-Mayorga, O.E. Acinonyx jubatus-Inspired Quadruped Robotics: Integrating Neural Oscillators for Enhanced Locomotion Control. *J. Biomimetics* **2024**, *9*, 318. [CrossRef] [PubMed]
22. Rico-Mesa, E.M.; Hernández-Riveros, J.A. Fuzzy Control with Central Pattern Generators for the Locomotion of Quadruped Robotic Systems. In *Communications in Computer and Information Science: LAWCN*; Riascos Salas, J.A., Cota, V.R., Villota, H., Betancur Vasquez, D., Eds.; Springer: Cham, Switzerland, 2024; pp. 69–91.
23. Kim, D.H.; Cho, J.; Park, J.H. Model Predictive Impedance Control and Gait Optimization for High-Speed Quadrupedal Running. *Appl. Sci.* **2025**, *15*, 8861. [CrossRef]
24. Rico, E.M.; Hernandez-Riveros, J.A. Analysis and Application of a Displacement CPG-Based Method on Articulated Frames, Advances in Computing. In *Communications in Computer and Information Science: Advances in Computing*; Solano, A., Ordoñez, H., Eds.; Springer: Cham, Switzerland, 2017; pp. 495–510.
25. Rico Mesa, E.M.; Hernández-Riveros, J.A. Modulation of Central Pattern Generators (CPG) for the Locomotion Planning of an Articulated Robot. In *Communications in Computer and Information Science: Applied Informatics*; Florez, H., Diaz, C., Chavarriaga, J., Eds.; Springer: Cham, Switzerland, 2018; pp. 321–334.
26. Rico Mesa, E.M.; Hernández-Riveros, J.A. Determination of the Central Pattern Generator Parameters by a Neuro-Fuzzy Evolutionary Algorithm. In *Advances in Emerging Trends and Technologies: ICAETT*; Botto-Tobar, M., León-Acurio, J., Díaz Cadena, A., Montiel Díaz, P., Eds.; Springer: Cham, Switzerland, 2020; pp. 518–530.
27. Rico Mesa, E.M.; Hernández-Riveros, J.-A. Handling the Transition in the Locomotion of an Articulated Quadruped Robot by Adaptive CPG. *J. IAENG* **2020**, *47*, 792–804.

Disclaimer/Publisher's Note: The statements, opinions and data contained in all publications are solely those of the individual author(s) and contributor(s) and not of MDPI and/or the editor(s). MDPI and/or the editor(s) disclaim responsibility for any injury to people or property resulting from any ideas, methods, instructions or products referred to in the content.